ACS Chemical Neuroscience

Article

N-(7-(1H-imidazol-1-yl)-2,3-dioxo-6-(trifluoromethyl)-3,4-dihydroquinoxalin-1(2H)-yl)benzamide - a new kainate receptor selective antagonist and analgesic: Synthesis, X-ray crystallography, structure-affinity relationships, in vitro and in vivo pharmacology

Stine Møllerud, Rie B. Hansen, Jakob S. Pallesen, Piero Temperini, Diletta Pasini, Jan Bornholdt, Birgitte Nielsen, Esmira Mamedova, Paulina Chalupnik, Ana V Paternain, Juan Lerma, Marta Diaz del Castillo, Jesper T. Andreasen, Karla Frydenvang, Jette Sandholm Kastrup, Tommy N. Johansen, and Darryl S. Pickering

ACS Chem. Neurosci., **Just Accepted Manuscript** • DOI: 10.1021/acschemneuro.9b00479 • Publication Date (Web): 17 Oct 2019

N-(7-(1*H*-imidazol-1-yl)-2,3-dioxo-6-(trifluoromethyl)-3,4-dihydroquinoxalin-1(2*H*)-yl)benzamide - a new kainate receptor selective antagonist and analgesic: Synthesis, X-ray crystallography, structure-affinity relationships, *in vitro* and *in vivo* pharmacology

Stine Møllerud,[a] Rie B. Hansen,[a] Jakob Pallesen,[a] Piero Temperini,[a] Diletta Pasini,[a] Jan Bornholt,[†, a] Birgitte Nielsen,[a] Esmira Mamedova,[a] Paulina Chalupnik,[b] Ana V. Paternain,[c] Juan Lerma,[c] Marta Diaz del Castillo,[a] Jesper T. Andreasen,[a] Karla Frydenvang,[a] Jette S. Kastrup,*[,a] Tommy N. Johansen*[,a] and Darryl S. Pickering*[,a]

[a]Department of Drug Design and Pharmacology, Faculty of Health and Medical Sciences, University of Copenhagen, DK-2100 Copenhagen, Denmark

[b]Department of Technology and Biotechnology of Drugs, Collegium Medicum, Jagiellonian University, PL 30-688 Kraków, Poland

[c]Institute of Neuroscience, CSIC-UMH, ES-03550 San Juan de Alicante, Spain

Abstract

Selective pharmacological tool compounds are invaluable for understanding the functions of the various ionotropic glutamate receptor subtypes. For the kainate receptors these compounds are few. Here we have synthesized 9 novel quinoxaline-2,3-diones with substitutions in the 7-position to investigate the structure-activity relationship at kainate and AMPA receptors. Compound **11** exhibited the highest binding affinity across GluK1-3 while having selectivity towards kainate *vs.* AMPA receptors. **11** potently inhibited glutamate evoked currents at homomeric GluK1 and GluK3 receptors in HEK293 cells with K_b values of 65 and 39 nM, respectively. The binding mode of **11** in the ligand binding domain of GluK1 was investigated by X-ray crystallography, revealing that **11** stabilizes the receptor in an open conformation, consistent with its demonstrated antagonism. Furthermore, **11** was tested for analgesic effects in the mouse tail flick test where it significantly increased tail flick latency at doses where NBQX was ineffective.

keywords: glutamate receptor, X-ray diffraction, electrophysiology, pain, analgesia, tail-flick

Introduction

The majority of fast excitatory neurotransmission in the mammalian central nervous system is mediated by glutamate acting through ionotropic glutamate receptors (iGluRs). This receptor family comprises the NMDA, AMPA, kainate and delta receptors.[1] The kainate receptors, consisting of the subunits GluK1-5, are located both at the pre- and postsynaptic membrane. Thus, in addition to a direct excitatory effect, kainate receptors are believed to modulate the activity of neuronal networks by facilitating or depressing neurotransmitter release.[2, 3] While AMPA and NMDA receptors have proven to be difficult therapeutic targets, the modulatory role of kainate receptors could potentially be a more suitable target as fine-tuning the balance of excitatory and inhibitory signaling could be more desirable than completely blocking the essential physiological functions of AMPA and NMDA receptors.

The physiological function of kainate receptors are less well understood compared to the AMPA and NMDA receptors. This is partially due to a relative lack of selective pharmacological tool compounds that can discriminate between AMPA and kainate receptors as well as between kainate receptor subtypes.[4] Extensive effort has been put into the design of kainate receptor selective antagonists, however only antagonists that selectively inhibit GluK1 receptors have been discovered so far.[5] Thus, there is an unmet need for subunit selective ligands for GluK2-5 to aid in the research on the individual functions of these receptor subunits in health and disease.

The quinoxaline-2,3-diones, such as 2,3-dioxo-6-nitro-1,2,3,4-tetrahydrobenzo[*f*]-quinoxaline-7-sulfonamide (NBQX; Figure 1), were among the first antagonists applied in non-NMDA receptor research. However, these compounds are not optimal for elucidating the functions of kainate receptors as they are also inhibitors of AMPA receptors.[4] Only few compounds with preferential binding at GluK3 or GluK2 have been reported. Some interesting compounds are: a *N*1-substituted quinoxaline-2,3-dione, LU97175 (**1**), which was reported to preferentially bind kainate receptor subunit GluK3 over GluK1 (>10 fold)[6] as well as the 6-substituted quinoxalinedione (**2**), which showed a slight preference for GluK3 over GluK1 (4-fold).[7] Recently we reported on a series of quinoxaline-2,3-diones substituted at the *N*1, 6- and 7-positions wherein compound **3** (*N*-(7-fluoro-2,3-dioxo-6-(trifluoromethyl)-3,4-dihydroquinoxalin-1(2*H*)-yl)-2-hydroxybenzamide) exhibited similar binding affinity as **1** with an 8-fold preferential binding at GluK3 over GluK1 receptors.[8]

In continuous efforts to identify useful ligands for functional characterization of kainate receptors, we have synthesized a series of quinoxaline-2,3-dione analogues with varying substituents in the 7-position and have pharmacologically characterized them with radioligand binding. Of this series

compound **11** showed the highest affinity at GluK3 and was further characterized by whole cell patch clamp in HEK293 cells expressing recombinant rat GluK1 or GluK3 receptors and *in vivo* for analgesic effects in the mouse tail flick test. Finally, to help understand the molecular interactions of this series of quinoxaline-2,3-dione we report a crystal structure of **11** in complex with the GluK1 ligand-binding domain (LBD).

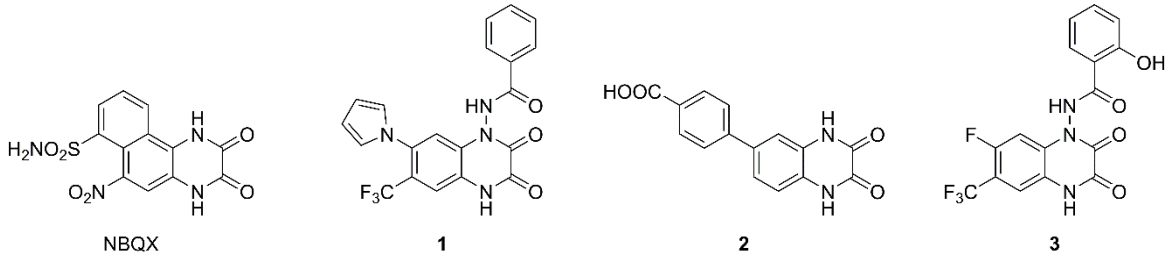

Figure 1. Chemical structures of selected quinoxaline-2,3-diones with antagonistic effect at AMPA/kainate receptors.

Results and Discussion

Medicinal chemistry

The first series of 7-substituted target compounds were based on a nucleophilic aromatic substitution (S_NAr) strategy (Scheme 1) starting from 1,5-difluoro-2-nitro-4-(trifluoromethyl)benzene (**4**). Compound **4** was easily transformed into the key intermediate **5** through a S_NAr reaction using benzhydrazide at room temperature followed by a second S_NAr reaction of the 5-fluoro substituent of **5** using selected *N*- and *S*-nucleophiles to afford benzohydrazides **6** – **9**. Three different transformations of the benzohydrazides **6** – **9** into the corresponding *N*1-benzamido-substituted quinoxaline-2,3-dione were investigated: **6** was converted to **10** in a one-pot procedure through acylation, reduction using iron in acetic acid and ring closure, analogous to a previously published strategy.[8] As an alternative to this strategy, benzohydrazides **7** and **9** were – in a two-step procedure – transformed into **11** and **13**, respectively, first through a Pd/C-catalyzed reduction of the nitro groups by polymethylhydrosiloxane (PMHS) based on a protocol developed by Rahaim and Maleczka,[9] followed by acylation and ring closure. As a variation of the second strategy, benzohydrazide **8** was converted to target compound **12** first reducing the nitro group through a Pd/C-catalyzed hydrogenation followed by acylation and ring closure. For the compounds investigated, all three methods seemed to be applicable and no preferred method was identified.

Scheme 1. Synthesis of Target Compounds 10 – 13.[a]

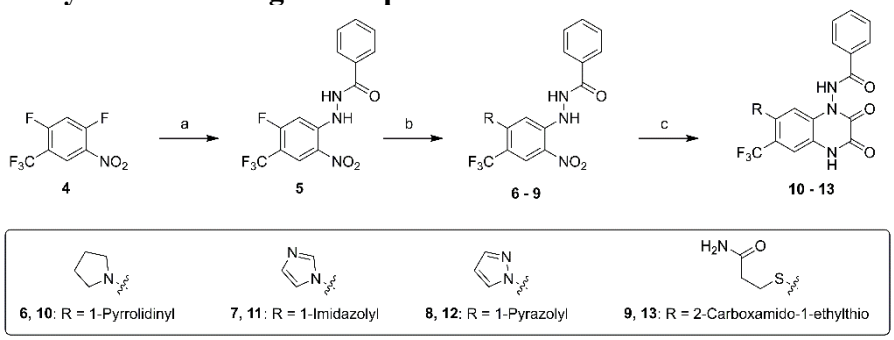

[a] Reagents and conditions: (a) benzohydrazide, DMSO rt, 30 min (b) appropriate nucleophile, DMSO, heat (c) ethyl chlorooxoacetate, pyridine, and then iron powder, AcOH, reflux (**10**); $Pd(OAc)_2$, KF, PHMS THF/H_2O, rt and then ethyl chlorooxoacetate, pyridine, DMF (**11** and **13**); Pd/C, H_2 (60 psi), EtOH and then ethyl chlorooxoacetate, pyridine, DMF (**12**).

Scheme 2. Synthesis of Target Compounds 14 – 25.[a]

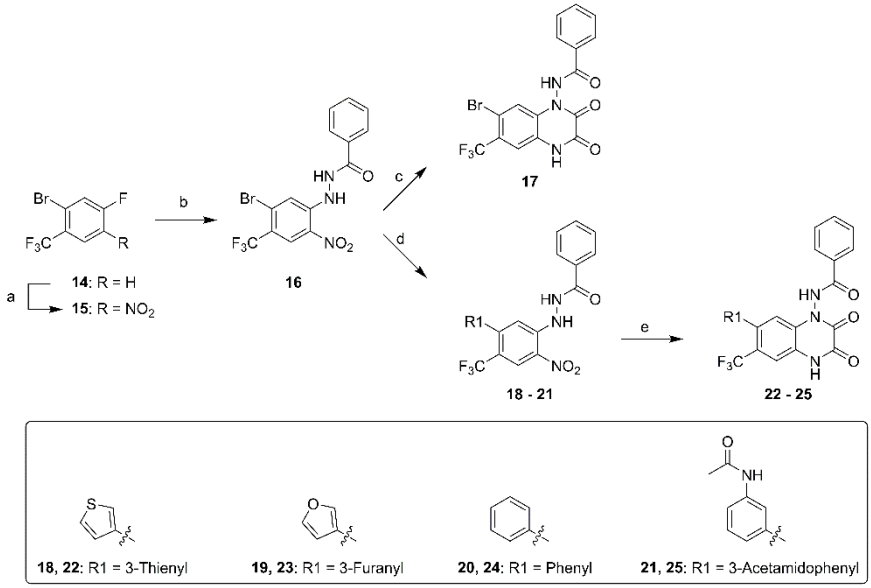

[a] Reagents and conditions: (a) KNO_3, H_2SO_4, 0 °C (b) benzohydrazide, DMSO, 100 °C (c) ethyl chlorooxoacetate, TEA, DCM and then iron powder, AcOH, reflux; (d) appropriate boronic acid, 2-aminobiphenyl-based second generation Buchwald precatalyst, K_3PO_4 (**18**-**20**); 3-acetamidobenzeneboronic acid, $Pd(dtbpf)Cl_2$, K_2CO_3 (**21**) (e) $Pd(OAc)_2$, KF, PHMS THF/H_2O, rt and then ethyl chlorooxoacetate, pyridine, DMF (**22** and **23**); ethyl chlorooxoacetate, pyridine, and then iron powder, AcOH, reflux (**24**); Pd/C, H_2, DMF and then ethyl chlorooxoacetate, pyridine, DMF (**25**).

The synthetic strategy for the second series of 7-substituted target compounds is shown in Scheme 2. First, 2-bromo-4-fluoro-trifluoromethylbenzene (**14**) was selectively nitrated as reported earlier[10] at 0 °C to give **15** in 37% yield. The fluoro atom of **15** was easily substituted by benzohydrazide at room temperature to give the key intermediate **16** which was converted to the 7-bromosubstituted quinoxaline-2,3-dione **17** *via* acylation, reduction using iron in acetic acid and ring closure. Attempts were made to use arylbromide **17** in Suzuki cross coupling reactions. Combinations of different

palladium sources and phosphine ligands, such as $Pd_2(dba)_3$, $Pd(OAc)_2$, $Pd(dtbpf)Cl_2$, $Pd(dppf)Cl_2 \cdot DCM$, the 2-aminobiphenyl-based second generation Buchwald precatalyst,[11, 12] *t*-Bu_3P, XPhos and SPhos, were investigated using different solvents and bases as well as conventional or microwave heating. In most cases, only unconverted starting material **17** could be seen even at high temperatures. Only when using the second generation Buchwald precatalyst[11] or $Pd(dppf)Cl_2 \cdot DCM$,[13] cross coupling products were observed, but it was not possible to optimize the conditions and to avoid the formation of side products. Instead, Suzuki cross coupling reactions using aryl bromide **16** and the second generation Buchwald precatalyst[11] or $Pd(dtbpf)Cl_2$, were straightforward and afforded **18** – **21** almost without the formation of side products. Compound **18** and **19** were converted to the corresponding quinoxalinediones **22** and **23**, respectively, using the Pd/C-catalyzed PMHS reduction followed by acylation and ring closure. The phenyl-substituted quinoxaline-2,3-dione **24** was prepared from **20** using the one-pot procedure through acylation, reduction using iron in acetic acid and ring closure, and finally, compound **25** was prepared from **21** through a Pd/C-catalyzed hydrogenation followed by acylation and ring closure.

In vitro pharmacology

The synthesized quinoxaline-2,3-diones were characterized in receptor binding studies at recombinant iGluRs (Table 1). For compound, **11**, which had the highest affinity at GluK1-3, the binding affinities were additionally determined at the soluble LBDs of GluK1, GluK3 and GluA2 yielding K_i values (mean ± SEM) of 43 ± 7 nM, 6.8 ± 2.5 nM and 670 ± 190 nM, respectively.

Additionally, to functionally characterize compound **11**, antagonist affinities (K_b) were determined by whole cell patch clamping. Compound **11**'s ability to inhibit glutamate evoked currents in cultured HEK293 cells expressing either homomeric rat GluK1 or GluK3 receptors was tested at a glutamate concentration (200 μM and 10 mM, respectively) close to the receptor EC_{50} values (212 μM and 14.4 mM, respectively) (Figure S1). **11** potently inhibited glutamate responses with similar apparent K_b values of 65 nM (95% confidence interval (CI): 52-82 nM) and 39 nM (95% CI: 26-60 nM) for GluK1(Q)$_{1b}$ and $GluK3_a$, respectively (Figure 2). This is in accordance with no statistically significant difference between the binding affinity at GluK1 and GluK3 ($P > 0.05$). Compared to compound **1**, where K_b values of 115 nM (GluK1) and 50 nM (GluK3)[8] were seen, **11** is comparably potent in inhibiting glutamate responses. This is in accordance with modest increases in the measured binding affinity of **11** (K_i: GluK1 = 166 nM, GluK3 = 78 nM) compared to **1** (K_i: GluK1 = 697 nM, GluK3 =

187 nM;[8]).These electrophysiological studies thus confirmed an antagonistic effect at homomeric GluK1 and GluK3 receptors.

Table 1: Binding Affinities of Quinoxaline-2,3-dione Analogues (K_i (μM), mean ± SEM)

Compound	GluK1	GluK2	GluK3	GluK5	GluA2	Native NMDAR
1[a]	0.697 ± 0.123	0.488 ± 0.058	0.187 ± 0.021	23.9 ± 4.0	1.52 ± 0.25	nd
10	4.19 ± 0.60	4.58 ± 0.38	3.50 ± 0.60	≈ 100	18.2 ± 1.2	5.5 ± 0.4
11	0.166 ± 0.011	0.523 ± 0.137	0.078 ± 0.011	5.20 ± 0.30	5.67 ± 0.25	9.6 ± 1.2
12	1.97 ± 0.23	1.68 ± 0.14	0.192 ± 0.038	10-50	10.1 ± 3.2	nd
13	0.606 ± 0.100	0.651 ± 0.149	0.181 ± 0.042	33.0 ± 3.6	4.53 ± 0.76	22 ± 3
17	1.61 ± 0.21	1.04 ± 0.20	0.460 ± 0.184	> 100	8.79 ± 1.47	> 10 [89%]
22	3.80 ± 1.00	2.45 ± 0.27	1.53 ± 0.40	57.8 ± 12.5	6.12 ± 0.67	1.5 ± 0.4
23	0.958 ± 0.076	1.69 ± 0.25	0.737 ± 0.022	43.0 ± 10.4	6.23 ± 0.51	4.2 ± 0.7
24	2.91 ± 0.32	2.07 ± 0.29	1.50 ± 0.30	≈ 100	8.16 ± 1.04	3.7 ± 0.5
25	1.29 ± 0.14	0.941 ± 0.092	0.360 ± 0.093	≈ 10	1.58 ± 0.17	nd

[a] ref [8], numbers in brackets is percentages of remaining specific radioligand binding at 10 μM quinoxalinedione derivative, nd: not determined.

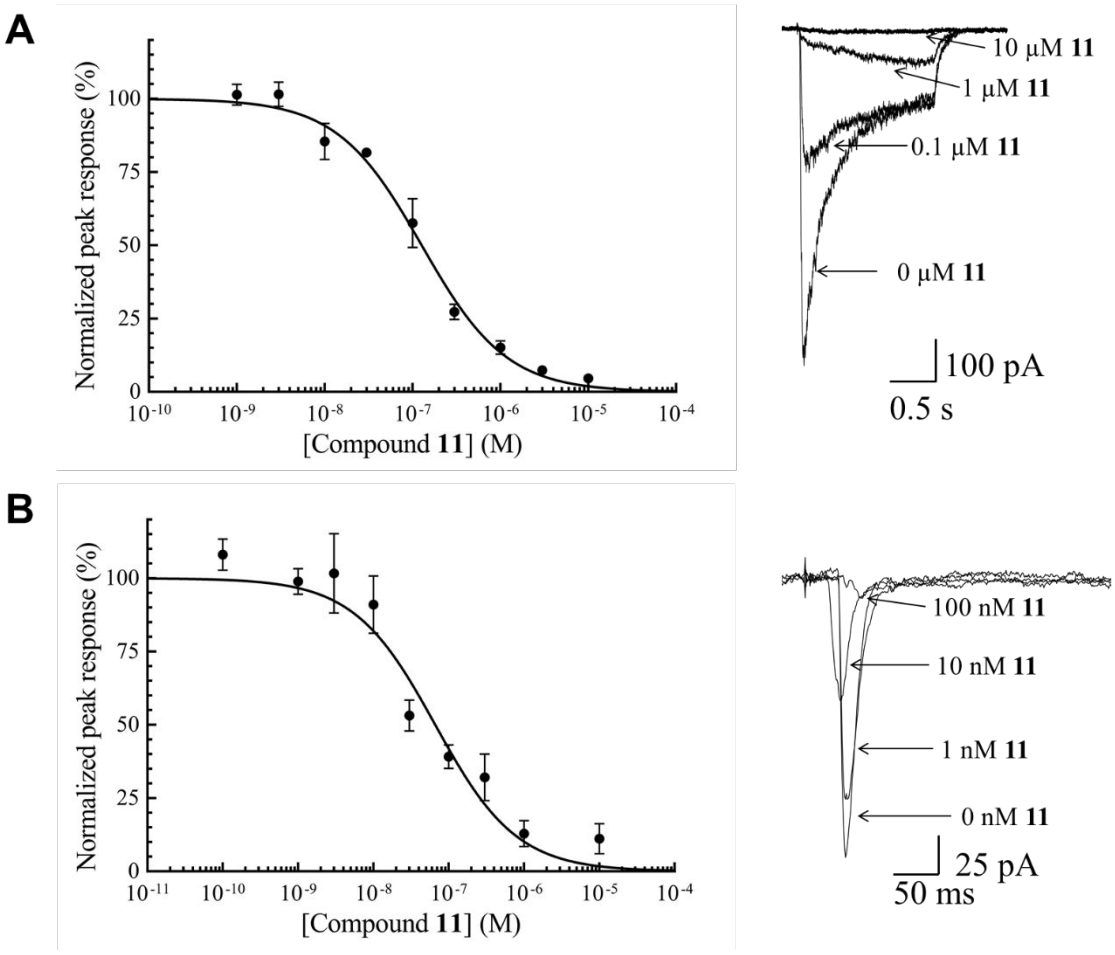

Figure 2. Antagonism of recombinant homomeric kainate receptors by compound 11. (A) Inhibition curve of **11** at GluK1(Q)$_{1b}$ receptors against 200 µM glutamate (n = 5-7 cells). K_b= 65 nM (95% CI: 52-82 nM). (B) Inhibition curve of **11** at GluK3$_a$ receptors against 10 mM glutamate (n = 3-11 cells). K_b= 39 nM (95% CI: 26-60 nM). Shown are mean ± SEM of the pooled, normalized data. Curves were constrained at 0% and 100% for bottom and top, respectively. Example traces for each curve are given to the right.

Structural analysis

The X-ray crystal structure of the GluK1-LBD in complex with **11** was determined at 2.3 Å resolution with clearly-defined electron density of **11** present in the binding site (Table 2, Figure 3A). The 2-one and 3-one of the quinoxaline-2,3-dione moiety of **11** make hydrogen bonds with Arg523 of GluK1-LBD (Figure 3A). The 3-one forms an additional contact to the backbone nitrogen atom whereas the 2-one has a hydrogen bond to a water molecule. The unsubstituted nitrogen of the

quinoxaline-2,3-dione forms a hydrogen bond with the backbone oxygen atom of Pro516 and the amide oxygen atom to a water molecule. Additionally, π–π stacking between the quinoxaline-2,3-dione moiety and Tyr489 (not shown) and potential π–π stacking of the benzamide substituent at the *N*1-position in the quinoxaline-2,3-dione with protein backbone of Gly688-Ser689 are observed. Finally, there is a sulfate ion present in the binding site as also previously observed in GluK1-LBD structures in complex with quinoxaline-2,3-diones[8, 14] as well as a putative chloride ion. The unsubstituted nitrogen atom of the imidazole substituent of **11** is probably protonated (complex crystallized at pH 4.5), making a salt bridge with the sulfate ion in the binding site possible. The chloride ion is located under the carbonyl carbon atom and *N*1 of the quinoxaline-2,3-dione of **11**.

The complex crystalized with one molecule in the asymmetric unit and forms a dimer with a symmetry related molecule (Figure 3B). The dimer interface involves both D1 and D2 lobe residues with a large buried surface area of 1278 Å^2 comparable to that observed in a structure with another quinoxaline-2,3-dione compound (1339 Å^2)[8]. Domain opening of the complex relative to a glutamate bound GluK1-LBD structure (PDB ID 2F36, molA) is 32.5°, which is in accordance with an antagonistic effect.[15]

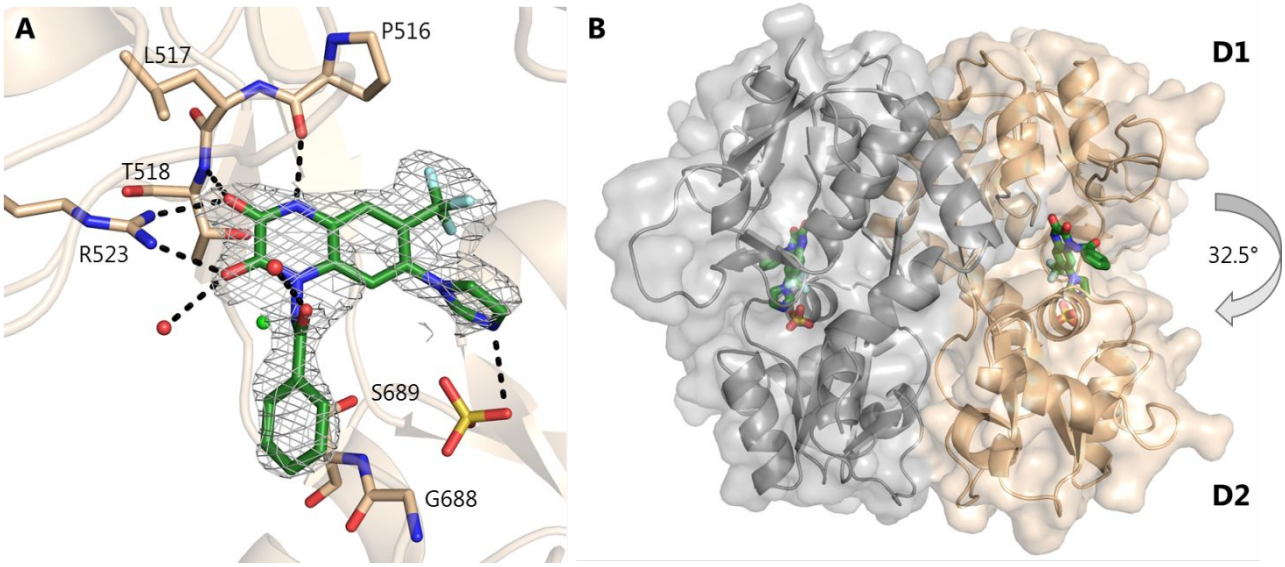

Figure 3. A) Interactions between **11** and GluK1-LBD (PDB ID 6SBT). The protein backbone is shown as cartoon and residues interacting with **11** are shown as beige sticks and **11** in stick representation with carbon atoms colored green. The sulfate ion located in the binding site is shown as sticks and water molecules interacting with **11** and a putative chloride ion are displayed as red and green spheres, respectively. Potential hydrogen bonds are shown as black dashed lines. A $2F_o$-F_c omit map carved around the ligand and contoured

at 1 sigma is shown in grey. B) Overall conformation of the GluK1-LBD dimer (molA grey, symmetry molA beige) shown as cartoon with surface representation. **11** (green) and sulfate are shown in stick representation. Domain opening is indicated by an arrow.

Table 2. Crystal Data, Data Collection and Structure Refinement of **11** in Complex with GluK1-LBD.

Crystal data	
Space group	*H*32
Unit cell: a,b,c (Å)	89.27, 89.27, 156.32
α, β, γ (°)	90.0, 90.0, 120.0
Wavelength (Å)	1.07227
Molecules in asymmetric unit of the crystal	1
Data collection	
Resolution (Å)[a]	44.64-2.30 (2.42-2.30)
Average redundancy	13.3 (12.8)
Completeness (%)	100 (100)
R_{merge} (%)[b]	11.1 (49.6)
I/σ(I)	6.2 (1.5)
CC1/2	0.99 (0.95)
Wilson B (Å^2)	27.1
Refinement	
R_{work}[c]/R_{free}[d](%)	20.5/24.9
Amino acid residues/**11**	249/1
Sulfate/chloride/glycerol/water	2/2/2/61
R.m.s. deviation bond length (Å)/angles (°)	0.002/0.53
Ramachandran outliers/favoured (%)	0.0/98.0
Rotamer outliers (%)/Cβ outliers (%)/Clash score	0.0/0.0/0.0
Average B-values (Å^2) for:	
Amino acid residues/**11**	49.6/42.5
Sulfate/chloride/glycerol/water	77.5/68.0/100.1/35.1

[a] Values in parenthesis correspond to outermost resolution shell. [b] R_{merge} is calculated as follows: $I_i(hkl)$ is the intensity of an individual measurement of the reflection with Müller indicies *hkl*, and I(*hkl*) is the intensity from multiple observations. $R_{merge} = \sum_{hkl}\sum_i \left| I_i(hkl) - I(hkl) \right| / \sum_{hkl}\sum_i \left| I_i(hkl) \right|$. [c] $R_{work} = \sum_{hkl} |F_{obs} - F_{calc}| / \sum_{hkl} |F_{obs}|$ where F_{obs} and F_{calc} are the observed and calculated structure factor amplitudes, respectively, for reflection *hkl*.[d] R_{free} is equivalent to R_{work}, but calculated with 5% of reflections omitted from the refinement process.

Structure-affinity relationships

In order to develop potential pharmacological tools for the characterization of kainate receptors, we have studied a series of *N*1-substituted quinoxaline-2,3-diones (all analogues of compound 1,[6, 8]; see Figure 1) with different substituents in the 7-position. Five of these compounds (**10** – **12**, **22** and **23**; Scheme 1 and 2) are 5-membered heterocyclic analogues of compound **1**, and three of these compounds (**11**, **12** and **23)** are equipotent or more potent as compared with starting compound **1**; compound **11** being the most potent compound within the series both at GluK1 and at GluK3 (Table

1), whereas compound **22** and, notably, compound **10** are less potent. Based on the X-ray structure of compound **11** co-crystallized with the GluK1-LBD, it is clear that these compounds all with 5-membered heterocyclic substituents most likely adopt conformations in which the heterocyclic substituents are close to orthogonal to the plane of the quinoxaline-2,3-dione similar to what is seen for compound **11**. These 5-membered heterocyclic substituents are similar in size and thus can easily be accommodated at GluK1 receptors (Figure 3A). The lack of affinity differences of these 5-membered heterocyclic substituents across GluK1-3 indicates that the GluK2 and GluK3 binding pockets can also accommodate such bulky substituents. Interesting loss of affinities (6-fold at GluK1, 9-fold at GluK2 and 19-fold at GluK3) were observed for compound **10** when compared with compound **1.** This loss of affinity may possibly be explained by electronic differences; the pyrrolidinyl of compound **10** being electron donating whereas the pyrrolyl of compound **1** being electron withdrawing. Therefore, an electron donating substituent at position 7, such as pyrrolidinyl, seems to reduce the ligand binding affinity.

The unsubstituted nitrogen atom of the imidazole substituent in the co-crystal structure of compound **11** was observed to form interaction with a sulfate ion located in the binding site. Most likely the sulfate ion will not be present physiologically and water-mediated contacts might be formed instead. Therefore, the basicity at this heteroatom – compared to the remaining heterocycles included in the present series – could contribute positively to the binding of compound **11** to the receptors.

Two compounds within the series (**24** and **25**) have larger 6-membered aromatic rings as substituents in the 7-position. Affinity data (Table 1) show that both these substituents are accepted by GluK1 - 3 receptors; compound **25** with an additional amido substituent being the more potent of the two. Compound **13**, also containing an amido substituent, but through a flexible side chain, is also well accepted by GluK1 - 3 receptors. Even though the GluK1-LBD co-crystal structure of compound **11** reveals the presence of residues capable of donating and accepting hydrogen bonds, the binding affinities of compound **13** and **25** seem to indicate that neither of the two amido substituents are involved in important receptor interactions through hydrogen bonding.

The series of compounds were also investigated at recombinant GluK5, GluA2 and at native NMDA receptors, the latter using [^{3}H]CGP 39653 as radioligand. At GluK5 receptors and at native NMDA receptors affinities between 1.5 and >100 μM were observed. Most interestingly, at GluK5 recombinant receptors the order of potency observed for compounds **1**, **10** and **11** follow the same trend as was seen at GluK1 and GluK3 receptors; compound **11** being 2.4 – 4.6-fold more potent

than compound **1** and compound **10** being 4 – 19-fold less potent than compound **1**. At GluA2 receptors, however, all compounds except compound **25** showed affinities within a narrow range (4.5 – 18 μM), illustrating that the structure-affinity relationships observed at GluK1 - 3 receptors could not be transferred to GluA2 receptors. Thus, with a K_i of 5.67 μM at GluA2 receptors compound **11** showed the largest discrimination between GluK3 and GluA2 (73-fold) compared to a corresponding 8-fold discrimination as seen for compound **1.** Compound **25** were the only new compound within the series with a GluA2 receptor affinity comparable to that of compound **1**. Interesting at GluA2 receptors, the 3-amido substituent of compound **25** apparently contributes positively to the binding of compound **25** as compared to compound **24**; compound **25** being 6-fold more potent than compound **24** at GluA2.

In vivo pharmacology

To assess the acute analgesic effect of **11** (0, 0.3, 1.2, 4.8 and 9.8 nmol i.t.) NMRI mice were tested for tail withdrawal response by the tail flick test. Animals were tested at baseline and 15, 30 and 60 min after drug administration. NBQX (8.0 nmol i.t.) and morphine (3.5 nmol i.t. or 5 mg/kg s.c.) treatment were included for comparison.

Tail flick test. Prior to injection a baseline response was determined for each treatment group. Intrathecal administration of **11** resulted in a dose-dependent increase in the tail flick latency in response to a noxious thermal stimulus applied to the tail (Figure 4A). The ANCOVA indicated a significant main effect of treatment ($F_{4,31} = 4.12$; $P < 0.001$) and time ($F_{2,63} = 21.53$; $P < 0.001$) but no treatment by time interaction ($F_{8,63} = 1.21$; $P = 0.31$). Pairwise comparisons within each time point showed that **11** significantly increased the latency for the two highest doses of **11** (4.8 and 9.8 nmol) at 15 min post drug administration and for the highest dose at 30 min compared to vehicle (15 min, 10.5 ± 0.5 s and 11.7 ± 1.6 s vs. 7.0 ± 1.2 s, $P < 0.05$ and $P < 0.001$; 30 min, 8.4 ± 0.8 vs. 4.6 ± 0.5 s, $P < 0.01$; n = 5-11). One mouse that was administered the highest dose of **11** had a minor paresis of the right hind paw at 15 and 30 min post drug administration; at 60 min, the paresis had resolved. This could be an adverse effect of **11**, but may also be due to the i.t. drug delivery.

For NBQX (8.0 nmol i.t.) there was a near-significant main effect of treatment ($F_{1,7} = 2.51$; $P = 0.072$), but not for time ($F_{2,16} = 2.04$; $P = 0.16$) or treatment by time interaction ($F_{2,16} = 2.45$; $P = 0.12$). Still the pairwise comparisons within each time point did show a significant increase the tail flick latency 30 min post drug administration when compared to vehicle treatment at the same time point (3.3 ± 0.4 s vs. 6.5 ± 0.2 s, $P < 0.01$, n = 5, Figure 4B). One mouse that was administered NBQX

had paralysis of the right hind limb after drug administration and was culled. This could be an adverse effect of NBQX[16], but may also be due to the i.t. drug delivery.

Morphine administration resulted in a significant main effect of treatment ($F_{2,20} = 5.28$; $P < 0.05$) and time ($F_{2,40} = 7.01$; $P < 0.01$) but no treatment by time interaction ($F_{4,40} = 0.69$; $P = 0.60$). Pairwise comparisons within each time point showed that i.t. administration of morphine (3.5 nmol) gave a significant increase in the tail flick latency at 30 min post drug administration when compared to vehicle treatment at the same time point (7.8 ± 0.8 s vs. 4.7 ± 0.5 s, $P < 0.05$, n = 7-11, Figure 4C). Subcutaneous administration of morphine (5 mg/kg) resulted in a significant increase in the tail flick latency 15 and 30 min post drug administration when compared to i.t. vehicle treatment (15 min, 10.4 ± 0.3 s vs. 7.0 ± 1.2 s, $P < 0.05$; 30 min, 8.4 ± 0.8 vs. 4.7 ± 0.5 s, $P < 0.01$; n = 6-11). One mouse that was administered i.t. morphine had a stiff upright tail and was excluded from the study. Two mice administered subcutaneous morphine were slightly hyperactive at 30 and 60 min post drug administration.

Although not statistically significant, it appears that the light isoflurane anaesthesia may affect the tail flick latency 15 min post drug administration where a minor increase in the latency is observed for the vehicle treated mice. This effect may possibly mask any minor analgesic effect of the lower doses of **11** and the effect of NBQX and i.t. morphine at 15 min.

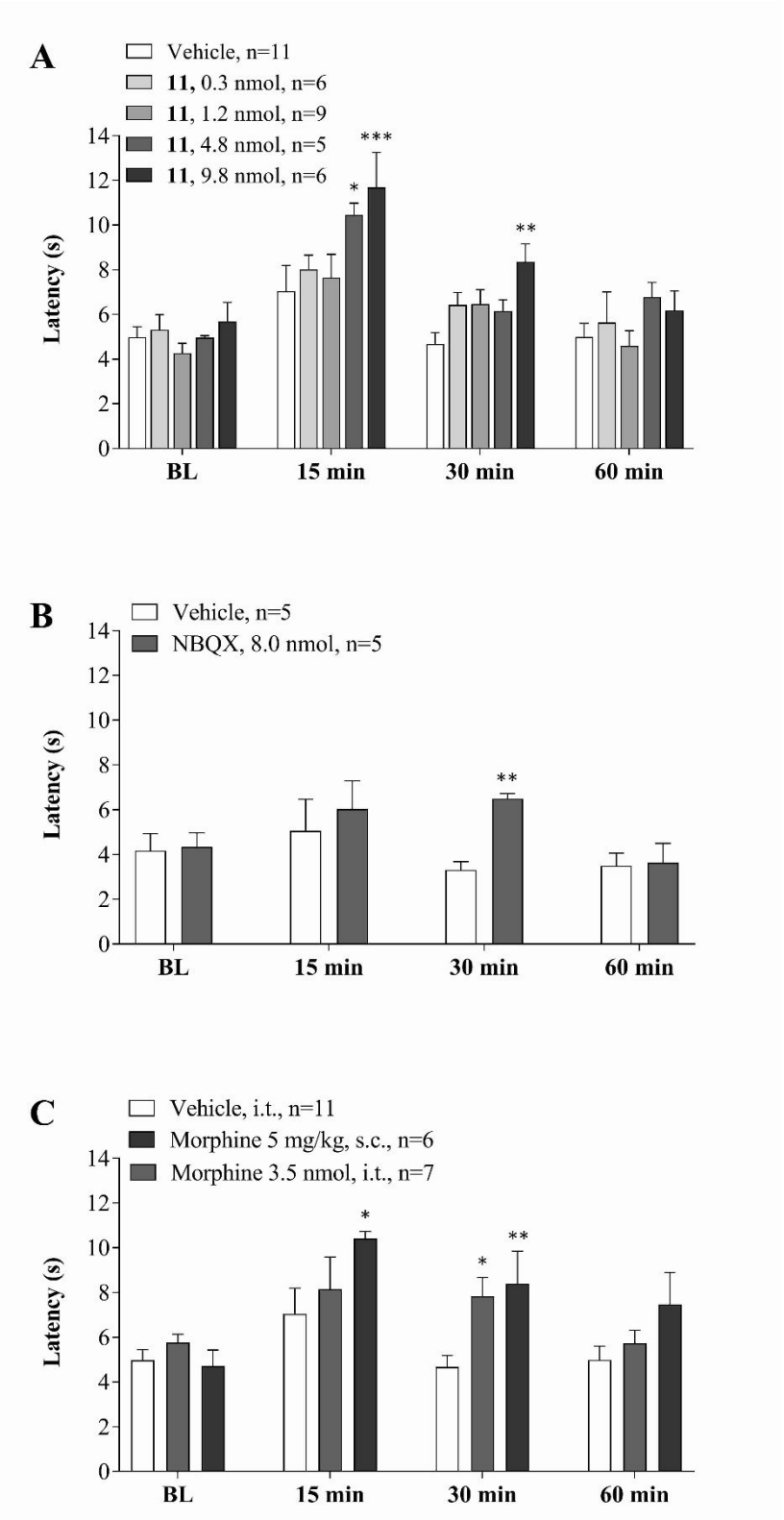

Figure 4. The effect of **11** on acute nociceptive behaviour in the mouse tail flick test. All drugs were administered after baseline (BL) latencies were obtained and the analgesic effect was assessed at 15, 30 and 60 min post drug administration. (A) **11** (0.3-9.8 nmol, 5 µl, i.t), (B) NBQX (8.0 nmol, 5 µl, i.t) and (C) morphine (3.5 nmol, 5 µl, i.t. or 5 mg/kg, s.c.). Data are presented as mean + SEM, n = 5-11 per group, *P < 0.05, **P < 0.01 and ***P < 0.001 compared to vehicle treatment at same time point (two-way RM ANCOVA followed by pairwise planned comparisons using Fisher's LSD).

Locomotor activity. ANOVA indicated a significant main effect of treatment ($F_{1,13} = 11.95$; $P < 0.01$, Figure 5) and time ($F_{8,104} = 17.11$; $P < 0.001$) but no treatment by time interaction ($F_{8,104} = 0.97$; $P = 0.46$). Pairwise comparisons within each time point showed that **11** significantly increased locomotor activity at the following time points: 10 min ($P < 0.001$), 15 min ($P < 0.01$), 20 min ($P < 0.05$) and 25 min ($P < 0.05$).

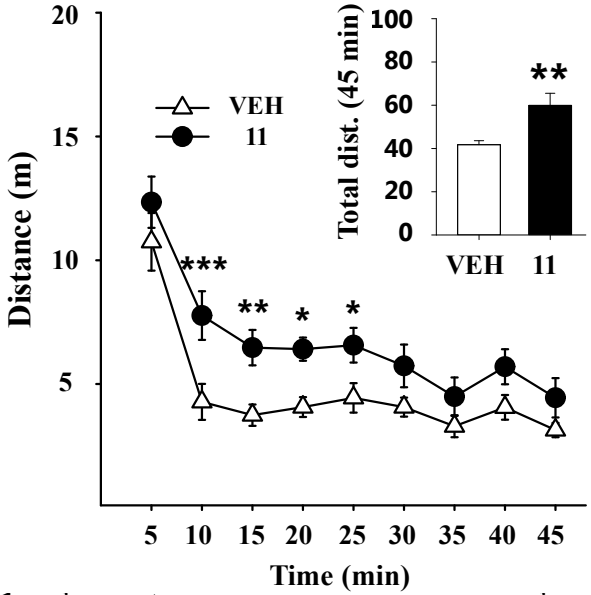

Figure 5. Effect of **11** on locomotor activity. **11** (9.8 nmol) caused an overall increase in locomotor activity ($F_{1,13} = 11.95$; $P < 0.01$), specifically increasing locomotor activity at 10 min ($P < 0.001$), 15 min ($P < 0.01$), 20 min ($P < 0.05$) and 25 min ($P < 0.05$), n = 7-8.

Rotarod test. The ANOVA showed no significant main effect of treatment ($F_{1,15} = 3.16$; $P = 0.10$, Figure 6), time ($F_{1,15} = 1.24$; $P = 0.28$) or treatment by time interaction ($F_{1,15} = 1.24$; $P = 0.28$). Pairwise comparison revealed no significant effect of **11** at the tested time points.

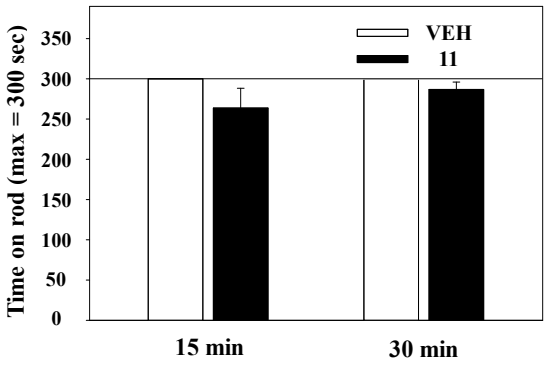

Figure 6. Effect of **11** (9.8 nmol) on motor coordination as measured with the rotarod test. **11** showed no significant effect on time spent on the rod, n = 9.

The canonical quinoxalinedione NBQX has been employed for many years in research as a non-NMDA iGluR competitive antagonist and has been previously demonstrated to show analgesic properties in mice.[16, 17] However, these early generation quinoxalinediones failed to proceed on to clinical trials due to problems of precipitation in the kidneys leading to nephrotoxicity.[18] One aim of our current study was thus to develop more potent quinoxalinedione analogues in the hopes that lower doses of compound may be better tolerated *in vivo* and still produce analgesia. Here we have preliminarily tested our lead compound (**11**) in the mouse tail flick test of acute pain where it was found to indeed show analgesia and to be more efficacious than NBQX. It is of note that in our radioligand binding experiments NBQX is 43-fold selective for GluA2 vs. GluK3 while **11** has the opposite selectivity, being 73-fold selective for GluK3 vs. GluA2. **11** is therefore a kainate receptor selective antagonist compared with NBQX. This supports the notion that the analgesic effects observed by the early generation quinoxalinediones were likely mediated via kainate receptors rather than AMPA receptors, consistent with a proposed role of kainate receptors in nociception.[19] Since **11** is non-selective amongst GluK1-3 we cannot know from our data which subtype of the kainate receptors is the predominant mediator of analgesia seen in this study. **11** had no adverse effects on motor coordination in the rotarod test, as previously observed for NBQX.[17] However, **11** was found to produce an increase in locomotor activity and further experiments are needed to examine this and to expand on the side effect profile of **11** as well as to determine its pharmacokinetic profile.

Conclusion

Based on the preference in binding at kainate receptors over AMPA receptors observed for compound **1** and our previous work investigating substitutions in the *N*1 and 6-position we have synthesized nine compounds with focus on varying the substituent in the 7-position. The quinoxaline-2,3-dione derivatives were tested in a radioligand binding assay and found to have relatively high binding affinity at kainate receptors. **11** showed the highest binding affinity across GluK1-3 along with the largest (73-fold) selectivity between GluA2 and GluK3. **11** potently inhibited glutamate evoked currents at homomeric GluK1 and GluK3 receptors recombinantly expressed in HEK293 cells with K_b values in the low nanomolar range. As a representative of the series of synthesized compounds **11** was crystallized with GluK1-LBD and induced a domain opening comparable to other antagonists. Finally, **11** showed analgesic effects in a mouse test of pain response at doses of 4.8 and 9.8 nmol, being more potent than NBQX. **11** could serve as a lead candidate for developing new potent and kainate receptor selective quinoxaline-2,3-diones.

Methods

Chemistry

Synthetic details can be found in the supporting information. Commercially available chemicals were used without any purification. Anhydrous reactions were carried out in oven or flame dried glassware. Dry solvents (DMF, THF and DCM) were dried using a solvent purification system. Thin layer chromatography was performed on TLC silica gel 60 F_{254} and compounds were visualized using UV light (254 nm). For flash column chromatography Merck silica gel 60 (0.063–0.200 mm) was used as the stationary phase. LC-MS was performed at an Agilent 1100 HPLC with an XBridge 3.5 μm C-18 column (100 × 4.6 mm) using a linear gradient elution from buffer A (H_2O:MeCN:HCOOH, 95:5:0.1) to buffer B (H_2O:MeCN:HCOOH, 5:95:0.1) over 10 min. Flow rate: 1.0 mL/min. The HPLC was coupled to a Hewlett Packard 1100 series mass spectrometer with an electrospray ionization source. Preparative HPLC was carried out on a Dionex ultimate 3000 system with binary pump, UV/VIS detector and 10 mL injection loop. The column was a Gemini® 5 μm NX-C18 110 Å, LC Column 250 × 21.2 mm. Appropriate linear gradient programs were set up using mobile phase A (H_2O:HCOOH, 100:0.1) and mobile phase B (H_2O:MeCN:HCOOH, 10:90:0.1) with a flow rate of 15 mL/min. ^{1}H-NMR was performed on a 400 MHz Bruker Avance III equipped with a 5 mm broad band probe at 400.09 MHz. Samples were dissolved in DMSO-d_6 or chloroform-*d* and analyzed at 300 K and referenced using DMSO at 2.50 ppm or chloroform at 7.26 ppm. ^{13}C-NMR was performed at 100.61 MHz using DMSO at 39.51 ppm or chloroform at 77.20 ppm as reference. Purity of the tested compounds was determined by analytical HPLC on an UltiMate HPLC system (ThermoScientific) consisting of a LPG-3400A pump (1.0 mL/min), a WPS-3000SL autosampler, and a DAD-3000D diode array detector using a Gemini-NX C18 column (4.6 × 250 mm, 3m, 110Å). Gradient elution (0 to 100% B (MeCN-H_2O-TFA 90:10:0.1) in solvent A (H_2O-TFA (100:0.1) over 10 min was used. Compounds were dissolved in MeCN. Data were acquired and processed using Chromeleon Software v. 6.80. All compounds tested had a purity at 254 and at 280 nm of at least 95%, unless otherwise stated.

Synthesis of target compound 11 and intermediate compounds 5 and 7.

***N*'-(5-Fluoro-2-nitro-4-(trifluoromethyl)phenyl)benzohydrazide 5.** Benzohydrazide (3.95 g, 29.0 mmol) was added to a stirred solution of **4** (6.50 g, 28.6 mmol) in dry DMSO (40 mL). The reaction mixture was stirred for 30 min at rt and under N_2 and then poured into a 0.1% aqueous $NaHCO_3$ solution (400 mL). Stirring was continued for 30 min. The precipitate was filtered, washed with H_2O and dried in vacuo to give **5** (9.34 g, 95%) as a yellow solid. ^{1}H-NMR (DMSO-d_6) δ 10.95 (s, 1H), 10.10 (s, 1H), 8.45 (d, J = 7.3 Hz, 1H), 7.98 (d, J = 7.0 Hz, 2H), 7.64 (t, J = 7.3 Hz, 1H), 7.55 (t, J = 7.2 Hz, 2H), 7.20 (d, J = 13.4 Hz, 1H). ^{13}C-NMR (DMSO-d_6) δ 166.56, 150.19, 132.67, 132.48, 129.00, 128.22, 127.84, 127.76, 102.59 (q, J = 27 Hz), 99.97.

***N*'-(5-(1*H*-Imidazol-1-yl)-2-nitro-4-(trifluoromethyl)phenyl)benzohydrazide 7.** Imidazole (817 mg, 12.0 mmol) was added to a stirred solution of **5** (1.029 g, 3.0 mmol) in dry DMSO (6 mL) under N_2. After heating at 100 °C for 45 min, the reaction mixture was poured into H_2O (60 mL) and aqueous KH_2PO_4 (1M, 2 mL), and stirred for 30 min. The beige precipitate formed was filtered, washed with H_2O and dried. Recrystallization from EtOH (40 mL) afforded **7** (970 mg, 83 %) as a yellow solid. ^{1}H-NMR (DMSO-d_6) δ 10.93 (s, 1H), 10.15 (s, 1H), 8.53 (s, 1H), 7.93 (d, J = 7.4 Hz, 2H), 7.84 (s, 1H), 7.61 (t, J = 7.3 Hz, 1H), 7.52 (t, J = 7,4 Hz, 2H), 7.40 (s, 1H), 7.25 (s, 1H), 7.08 (t, J = 1.1 Hz, 1H). ^{13}C-NMR (DMSO-d_6) δ 166.57, 147.83, 141.12, 138.54, 132.67, 132.42, 130.12, 129.52, 129.02, 128.14, 126.98, 123.32 (q, J = 270 Hz), 122.18, 116.16, 113.64 (q, J = 32 Hz).

***N*-(2,3-Dioxo-7-(1*H*-imidazol-1-yl)-6-(trifluoromethyl)-3,4-dihydroquinoxalin-1(2*H*)-yl)-benzamide 11.** $Pd(OAc)_2$ (3 mg, 0.014 mmol,) and **7** (110 mg, 0.32 mmol,) were dissolved in freshly distilled dry THF (5 mL) under N_2. Aqueous KF (0.048 g, 0.84 mmol, in 0.8 mL degassed H_2O) was added, followed by dropwise addition of PMHS (0.1 mL, 1.68 mmol). The reaction was stirred at rt for 3 h, Et_2O (10 mL) was added, and the stirring continued for 5 min. The layers were separated and the aqueous layer was extracted with Et_2O (2 × 20 mL). The combined organic phases were filtered through Celite flushing with EtOAc. The filtrate was dried with $MgSO_4$, filtered and concentrated in vacuo. The residue was dissolved in dry DMF (4 mL), ethyl chlorooxoacetate (0.035 mL, 0.32 mmol) and pyridine (0.067 mL, 0.83 mmol) was added and the reaction mixture was stirred under N_2 at rt for 1h and at 100 °C overnight. The crude product was purified by preperative HPLC. Appropriate fractions were concentrated and freeze-dried to give **11** as a white solid (93 mg, 70 %). ^{1}H-NMR (DMSO-d_6) δ 12.93 (s, 1H), 11.90 (s, 1H), 8.81 (s, 1H), 8.05 (d, J = 7.6 Hz, 2H), 7.88 (d, J = 8.1 Hz,

2H), 7.75 (s, 1H), 7.67 (t, J = 7.2 Hz, 1H), 7.60 – 7.53 (m, 3H). 13C-NMR (DMSO-d6) δ 165.52, 162.35, 153.74, 132.85, 131.49, 130.98, 128.63, 128.17, 125.19, 122.98.

Crystallization

Rat GluK1-LBD was expressed and purified as previously described.[20] In short, the LBD construct was expressed in the *E. coli* cell line Origami 2. The construct contains an *N*-terminal His fusion tag (leaving a glycine after tag removal) and the protein was purified by nickel affinity chromatography on a HisTrap column followed by ion exchange and size exclusion chromatography. **11** was dissolved in protein buffer (10 mM HEPES pH 7.0, 20 mM NaCl) and pH was increased to approximately 9 with concentrated NaOH to increase solubility before mixing with GluK1-LBD. Solid **11** was added to saturate the solution and protein-ligand solution was equilibrated for 3 h at 6°C prior to setup.

GluK1-LBD in complex with **11** was crystallized by the hanging drop vapor diffusion method at 6°C. Drops consisted of 1 µL reservoir solution and 1 µL complex solution (4.0 mg/mL GluK1-LBD and saturated **11** with excess of solid **11**). Volume of reservoir solution was 0.5 mL and crystals grew within one week from set up. The crystal used for data collection was achieved using reservoir solution containing 20% PEG4000, 0.3 M lithium sulfate, 0.1 M phosphate-citrate, pH 4.5.

X-ray data collection and processing

Crystals were soaked in cryo-buffer (reservoir solution containing 20% glycerol) and flash cooled in liquid nitrogen. X-ray diffraction data were collected at the ID29 beamline (ESRF, Grenoble, France) at a wavelength of 1.07227 Å to 2.3 Å resolution. Data processing was performed with XDS[21] and SCALA within the CCP4i suite of programs.[22] Molecular replacement using PHASER (implemented in CCP4i;[23]) was performed using individual D1 and D2 lobes of PDB entry 4QF9 (molA) as search models. Automated model building was initially performed using AutoBuild in PHENIX.[24] Next, **11** coordinates were created in Maestro [Maestro version 10.7, Schrödinger, LLC, New York, NY, 2016], geometry optimized [MacroModel 11.3, Schrödinger, LLC New York, NY, 2016]] and fitted into the electron density in the ligand binding site. A restraint file for **11** was generated with eLBOW keeping geometry obtained in Maestro.[25] The structure was refined in PHENIX using isotropic B factors, TLS and riding hydrogen atoms. The structure was manually inspected and corrected in COOT[26] between refinement steps.

Structure analysis

Domain opening was calculated relative to the structure of the fully closed structure of GluK1-LBD in complex with glutamate (PDB entry 2F36, molA) using the DynDom server.[27] Buried surface areas were calculated using the PISA server[28] and figures were prepared using PyMOL [The PyMOL Molecular Graphics System, version 1.8.6.1, Schrödinger, LCC].

Radioligand binding assays

Native NMDA receptors. Binding at native NMDA receptors was carried out as previously detailed[29] in rat brain synaptosomal membranes which had been washed four times in ice-cold 50 mM Tris-HCl buffer, pH 7.4, containing 2.5 mM $CaCl_2$ on the day of assaying and using 2 nM [^{3}H]CGP 39653. The final pellet was resuspended in ice-cold buffer to an approximate concentration of 0.4–0.5 mg of protein/mL. The binding was carried out in 96-wells plates in a total volume of 250 µL and equilibrated at 0 °C for 60 min before rapid filtration through GF/C filters (Perkin-Elmer Life Sciences), using a 96-well Packard FilterMate cell harvester, and three washes with 250 µL of ice-cold binding buffer. To the dried filters was added 30 µL/well of Microscint scintillation fluid (Perkin-Elmer Life Sciences), and the amount of filter bound radioactivity was quantified in a Packard TopCount microplate scintillator counter. Nonspecific binding was determined using 1.0 mM Glu.

Full length receptors. Ligand binding affinities at recombinant rat homomeric GluA2, GluK1-3 and GluK5 were determined as previously detailed.[30-32] In short, ligands were diluted in assay buffer (GluA2: 50 mM Tris-HCl, 100 mM KSCN, 2.5 mM $CaCl_2$ pH 7.2 at 4 °C; GluK1-3,5: 50 mM Tris-HCl pH 7.1 at 4 °C), mixed with *sf9* insect cell membranes expressing the respective receptors and radioligand (GluA2: [^{3}H]-(*RS*)-AMPA (57.5 Ci/mmol; PerkinElmer, Waltham, MA), GluK1: [^{3}H]-(*S*)-NF608 (16.3 Ci/mmol)[30], GluK2,3,5: [isopropenyl-^{3}H]-kainic acid (43.6-47.2 Ci/mmol; PerkinElmer) in a total volume of 0.25 mL followed by 2h equilibration at 4 °C. GluK1-3 assays were filtered through GF/B-type glass fiber filters in microtitre plate format (UniFilter-96, PerkinElmer) and washed twice with ice-cold assay buffer on a FilterMate manifold (PerkinElmer). The filters were dried at 70 °C for 1 h and 50 µL/well Microscint 20 (PerkinElmer) was added. Radioactivity was detected with a TopCounter (PerkinElmer). GluA2 and GluK5 assays were filtered on GF/C type filters using Millipore 12-well filtration manifolds (Merck Life Science, Denmark) and washed twice with ice-cold assay buffer. Filters were placed in pony vials (PerkinElmer), 3 mL Ultima Gold scintillation fluid (PerkinElmer) added and DPM determined using a TriCarb 2900 scintillation counter (PerkinElmer).

Soluble ligand binding domain constructs. Binding to GluA2-LBD (50 ng protein/tube), GluK1-LBD (50 ng/tube) and GluK3-LBD (250 ng/tube) was conducted essentially as previously described.[33, 34] LBD assay buffers are the same as for full length receptor binding but additionally contain 10% (v/v) glycerol. Experiments were performed at 4 °C and bound and free radioligand were separated by filtration onto 0.22 μM mixed cellulose ester filters (Tisch Scientific, North Bend, OH) on a 12-well Millipore filtration manifold, washing twice with 1 mL ice-cold assay buffer. Filters were dried, then solubilized in 2 mL Filter Count scintillation fluid (PerkinElmer) and radioactivity determined by liquid scintillation counting using a TriCarb 2900 scintillation counter.

Binding data analysis. All competition curves ($n \geq 3$ per ligand) were determined in triplicate at 12–16 ligand concentrations. Data were analyzed using GraphPad Prism 6 (GraphPad Software, San Diego, CA) to determine ligand affinity (K_i) and Hill coefficient (n_H) using the one-site K_i and four-parameter logistics equations, respectively.

Electrophysiology

Cell culturing and transfection. HEK293 cells were maintained in Dulbecco's modified eagle medium supplemented with fetal bovine serum and penicillin/streptomycin. Cells were seeded on poly-*D*-lysine-coated coverslips and transiently transfected with 3 μg rat GluK1(Q)$_{1b}$ or 5 μg rat GluK3$_a$ cDNA (in pCis vector) using 2 μL lipofectamine (Invitrogen, CA) per transfection. Cells were co-transfected with 1 μg GFP for visualization of transfected cells and used 24-72 h post transfection.

Recording procedure. Membrane currents were recorded using the patch-clamp technique under whole-cell configuration. Patch pipettes had resistances of 3–5 MΩ. Currents were filtered at 10 kHz (two-pole Butterworth filter, −12 db/octave) and transferred to a personal computer for analysis. Extracellular solution contained (in mM): 140 NaCl, 2.5 KCl, 1.8 $CaCl_2$, 10 HEPES, 15 glucose, 1 $MgCl_2$, pH 7.3-7.4. Pipette solution (in mM): 130 $CsMeSO_4$, 4 NaCl, 10 HEPES, 10 TEA, 1 EGTA, 5 Qx314 bromide (Sigma Chemical, MO), 2 ATP, 0.5 GTP, pH 7.3, 290 mOsm. (*S*)-glutamate was diluted from stock solutions on the day of experiment. A 25 mM solution of **11** in DMSO was prepared and stored at -20 °C. On the day of experiment **11** was diluted and added to (*S*)-glutamate solutions (maximal final DMSO concentration: 0.04%). All experiments were performed at a holding potential of -60 mV and at room temperature. The cells were rapidly perfused using a linear array of 7 glass tubes and rapid change (< 2 ms) between solutions was controlled by a motor. K_b values were

determined using glutamate concentrations (GluK1: 200 μM, GluK3: 10 mM) near the respective EC_{50} values (212 μM, 14.4 mM, respectively. Supplementary Information, Figure S1). **11** was pre-applied for 20-30 seconds before the same concentration of **11** was co-applied with glutamate. Data were collected and pooled from 27 cells for GluK1$(Q)_{1b}$ and 29 cells for $GluK3_a$.

Electrophysiology data analysis. Data were displayed using pClamp software (Axon Instruments, Foster City, CA, USA), and responses were normalized to a saturating (GluK1: 10 mM, GluK3: 100 mM) glutamate response (= 100% response). Data were analyzed using GraphPad Prism 6 (GraphPad Software, San Diego, CA) to determine IC_{50} and Hill slope (4-parameter logistic equation). IC_{50} values of the pooled, normalized curves were converted to K_b values using the modified Cheng-Prusoff equation.

In vivo pharmacology

Animals. A total of 90 six week old male NMRI mice (Envigo, Venray, The Netherlands) were included in the study. The animals were housed in groups in individually ventilated GM500+ cages (524 cm^2) at a 12-hour light-dark cycle (lights on at 07:00 AM) in a temperature (20-24 ˚C) and humidity controlled environment. Upon arrival, animals were left to acclimatize for a minimum of one week prior to initiation of experiments. They were provided with Tapvei 2HV wood-chip bedding material (Harjumaa, Estonia) and allowed free access to water and standard diet (Altomin 1314; Brogaarden, Lynge, Denmark) except during behavioural testing, which was conducted between 9 am and 4 pm. For environmental enrichment, mice were provided with paper ropes, an S-brick (Tapvei, Harjumaa, Estonia), a red translucent shelter and corn hidden in the bedding. The experiment was approved by the Danish Animal Experiments Inspectorate, Ministry of Environment and Food (License no. 2012-15-2934-00165, C3) and conducted under the guidelines of the International Association for the Study of Pain.[35]

Drug treatment. **11** (synthesised in house at the Department of Drug Design and Pharmacology, University of Copenhagen, Denmark), NBQX (Tocris Bioscience, Bristol, United Kingdom) and morphine hydrochloride (10 mg/ml, Skanderborg Produktionsapotek, Denmark) were dissolved/diluted in 4% DMSO/10 mM NaH_2PO_4 (pH = 8.0) and administered intrathecally (i.t., 26-gauge needle) at the lumbar enlargement of mice as a single bolus injection of 5 μl. Morphine administered subcutaneously (s.c.) was diluted in sterile saline. The highest dose of **11** (9.8 nmol) and

s.c. morphine was assessed in a separate experiment, however, as no significant differences were found in baseline tail flick latencies the data was pooled.

Tail flick test. The reflex response to a noxious thermal stimulus was measured in normal uninjured NMRI male mice using the tail flick test. Mice were placed in cylindrical Plexiglas test boxes on a framed glass pane (Ugo Basile Inc., Comerio, Italy) and habituated for approximately 45 minutes. A radiant heat source (Plantar Test, Ugo Basile Inc., Comerio, Italy) was focused on the ventral surface of the tail ⅓-¼ down from the base of the tail. The apparatus was calibrated to give a baseline tail flick latency of approximately 4–6 s (20 s cut-off) and the tail flick latency was measured to the nearest 0.1 s. Before drug testing mice were acclimatised to the test chamber on two separate days and a baseline measurement performed to familiarize the mice with the testing procedure. A baseline measurement (two measurements separated by 5 min) was made just prior to the drug test. Mice were lightly anaesthetized with isoflurane (Baxter A/S, Allerød, Denmark) administered either drug or vehicle and the tail flick latency measured 15, 30 and 60 min post drug administration. The experimenter was blinded to drug treatment.

Tail flick data analysis. Data were analyzed with a two-way repeated measure analysis of covariance (RM-ANCOVA) with baseline as covariate, treatment as independent factor and time as repeated measure followed by pairwise planned comparisons using Fisher's LSD. One-way ANOVA followed by Tukey's multiple comparisons test was used to compare baseline tail flick latencies prior pooling of the data. For all statistical analyses, a probability value of $P < 0.05$ was considered significant.

Spontaneous activity - locomotor activity (LA) test. Mice (n = 7-8) were individually placed for 30 minutes in transparent cages (L: 37 cm x W: 21 cm x H: 15 cm) with a thin layer of bedding. Locomotor distance was automatically recorded by a camera mounted above the arenas and stored on a computer equipped with Ethovision XT (Noldus, Holland).

Motor coordination - rotarod test. Motor function was evaluated using an accelerating rotarod (MedAssociates, Inc., VT). The rotarod (3.2 cm diameter) speed was increased from 4 to 40 rpm over a 300 s period with the minimum time possible to spend on the rod designated as 0 s and the maximum cut-off time set at 310 s. Mice (n = 9) were tested 15 and 30 minutes after treatment. When an animal

fell off the rotating drum, a photobeam was automatically broken to record the amount of time spent on the rotating rod.

Locomotor and coordination data analysis. Data were analyzed with a two-way repeated measure analysis of variance (RM-ANOVA) with treatment as independent factor and time as repeated measure followed by pairwise planned comparisons using Fisher's LSD. To ensure normality and variance homogeneity, which is required for ANOVA/ANCOVA, data were log-transformed before statistical analysis, but displayed graphically on the original scale.

ASSOCIATED CONTENT

Supporting Information.

The Supporting Information available free of charge on the ACS Publication website at DOI: XXX, includes:

Synthesis and characterization of compounds; Figure S1, Glutamate concentration-response curves of transfected HEK293 cells (PDF)

Molecular formula strings (CSV)

Accession Codes

The structure of compound **11** in GluK1-LBD is deposited in the protein data bank (PDB ID 6SBT). Authors will release the atomic coordinates and experimental data upon article publication.

Author Information

Corresponding Authors
*D.S.P. on pharmacology: Email: picker@sund.ku.dk Phone: +45 35334342.
*T.N.J. on chemistry: E-mail: tnj@sund.ku.dk. Phone: +45 35336412.
*J.S.K. on crystallography: E-mail: jsk@sund.ku.dk . Phone: +45 35336486.

ORCID
Karla Frydenvang: 0000-0002-5823-3478
Darryl S. Pickering: 0000-0001-8687-6094
Jette Sandholm Kastrup: 0000-0003-2654-1510
Tommy N. Johansen: 0000-0001-5918-0833
Stine Møllerud: 0000-0001-6828-8539

Present Address
† J.B.: LEO Pharma A/S, Industriparken 55, DK-2750 Ballerup, Denmark.

Author Contributions
Design and synthesis: J.P., J.B., E.M., P.C., and T.N.J. Pharmacology: S.M., P.T., D.P., B.N., A.V.P., J.L., and D.S.P. In vivo studies: R.B.H., M.D.C., and J.T.A. Crystallography: S.M., K.F., and J.S.K. All authors interpreted data and contributed to data analysis. All authors have given approval to the final version of the manuscript.

Notes
The authors declare no competing financial interest.

Acknowledgements
Heidi Peterson is thanked for help with expression and purification of the ligand-binding domain of GluK1. ESRF, Grenoble, France is thanked for providing beam time.
This research was generously supported by: the Lundbeck Foundation (S.M., D.S.P., K.F., and J.S.K.), GluTarget (J.B., T.N.J.), Danscatt (S.M., K.F., J.S.K.), European Union Horizon 2020 Research and Innovation Program under the Marie Skłodowska-Curie grant agreement No. 642720 (M.D.C).

Abbreviations used
AMPA, α-amino-3-hydroxy-5-methyl-4-isoxazolepropionic acid); GluK1-LBD, ligand-binding domain of GluK1; iGluRs, ionotropic glutamate receptors; i.t., intrathecal; LBD, ligand-binding domain; LU 97175, 1-benzamido-7-pyrrol-1-yl-6-trifluoromethylquinoxaline-2,3-(1H,4H)-dione; NBQX, 2,3-dioxo-6-nitro-1,2,3,4-tetrahydrobenzo[f]-quinoxaline-7-sulfonamide; [^{3}H]NF608, (S)-2-amino-3-(6-[^{3}H]-2,4-dioxo-3,4-dihydrothieno[3,2-d]pyrimidin-1(2H)-yl)-propanoic acid; NMDA, N-methyl-*D*-aspartate; s.c., subcutaneous.

References

1. Traynelis, S. F.; Wollmuth, L. P.; McBain, C. J.; Menniti, F. S.; Vance, K. M.; Ogden, K. K.; Hansen, K. B.; Yuan, H.; Myers, S. J.; Dingledine, R. Glutamate receptor ion channels: structure, regulation, and function. *Pharmacol Rev* **2010,** 62, 405-96.
2. Evans, A. J.; Gurung, S.; Henley, J. M.; Nakamura, Y.; Wilkinson, K. A. Exciting Times: New Advances Towards Understanding the Regulation and Roles of Kainate Receptors. *Neurochem Res* **2019,** 44, 572-584.
3. Lerma, J.; Marques, J. M. Kainate receptors in health and disease. *Neuron* **2013,** 80, 292-311.
4. Jane, D. E.; Lodge, D.; Collingridge, G. L. Kainate receptors: pharmacology, function and therapeutic potential. *Neuropharmacology* **2009,** 56, 90-113.
5. Larsen, A. M.; Bunch, L. Medicinal chemistry of competitive kainate receptor antagonists. *ACS Chem Neurosci* **2011,** 2, 60-74.
6. Loscher, W.; Lehmann, H.; Behl, B.; Seemann, D.; Teschendorf, H. J.; Hofmann, H. P.; Lubisch, W.; Hoger, T.; Lemaire, H. G.; Gross, G. A new pyrrolyl-quinoxalinedione series of non-NMDA glutamate receptor antagonists: pharmacological characterization and comparison with NBQX and valproate in the kindling model of epilepsy. *Eur J Neurosci* **1999,** 11, 250-62.
7. Demmer, C. S.; Rombach, D.; Liu, N.; Nielsen, B.; Pickering, D. S.; Bunch, L. Revisiting the Quinoxalinedione Scaffold in the Construction of New Ligands for the Ionotropic Glutamate Receptors. *ACS Chem Neurosci* **2017,** 8, 2477-2495.
8. Pallesen, J. S.; S, M.; Frydenvang, K.; Pickering, D. S.; Bornholdt, J.; Nielsen, B.; Pasini, D.; Han, L.; Marconi, L.; Kastrup, J. S.; Johansen, T. N. N1-Substituted Quinoxaline-2,3-diones as Kainate Receptor Antagonists: X-ray Crystallography, Structure-Affinity Relationships and in vitro Pharmacology. *ACS Chem Neurosci* **2019**.
9. Rahaim, R. J., Jr.; Maleczka, R. E., Jr. Pd-catalyzed silicon hydride reductions of aromatic and aliphatic nitro groups. *Org Lett* **2005,** 7, 5087-90.
10. Cooper, D. G. F., I. T.; Garzya, V.; Jin, J.; Louchart, Y.; Walker, G.; Wyman, P. A. Benzimidazoles which have activity at m1 receptor and their uses in medicine. 2007.
11. Kinzel, T.; Zhang, Y.; Buchwald, S. L. A new palladium precatalyst allows for the fast Suzuki-Miyaura coupling reactions of unstable polyfluorophenyl and 2-heteroaryl boronic acids. *J Am Chem Soc* **2010,** 132, 14073-5.
12. Konig, M.; Reith, L. M.; Monkowius, U.; Knor, G.; Bretterbauer, K.; Schoefberger, W. Suzuki-Miyaura cross-coupling reaction on copper-trans-A(2)B corroles with excellent functional group tolerance. *Tetrahedron* **2011,** 67, 4243-4252.
13. Jung, D.; Shimogawa, H.; Kwon, Y.; Mao, Q.; Sato, S.; Kamisuki, S.; Kigoshi, H.; Uesugi, M. Wrenchnolol derivative optimized for gene activation in cells. *J Am Chem Soc* **2009,** 131, 4774-82.
14. Demmer, C. S.; Moller, C.; Brown, P. M.; Han, L.; Pickering, D. S.; Nielsen, B.; Bowie, D.; Frydenvang, K.; Kastrup, J. S.; Bunch, L. Binding mode of an alpha-amino acid-linked quinoxaline-2,3-dione analogue at glutamate receptor subtype GluK1. *ACS Chem Neurosci* **2015,** 6, 845-54.
15. Møllerud, S.; Frydenvang, K.; Pickering, D. S.; Kastrup, J. S. Lessons from crystal structures of kainate receptors. *Neuropharmacology* **2017,** 112, 16-28.
16. Lutfy, K.; Cai, S. X.; Woodward, R. M.; Weber, E. Antinociceptive effects of NMDA and non-NMDA receptor antagonists in the tail flick test in mice. *Pain* **1997,** 70, 31-40.

17. Blackburn-Munro, G.; Bomholt, S. F.; Erichsen, H. K. Behavioural effects of the novel AMPA/GluR5 selective receptor antagonist NS1209 after systemic administration in animal models of experimental pain. *Neuropharmacology* **2004,** 47, 351-62.
18. Turski, L.; Schneider, H. H.; Neuhaus, R.; McDonald, F.; Jones, G. H.; Lofberg, B.; Schweinfurth, H.; Huth, A.; Kruger, M.; Ottow, E. Phosphonate quinoxalinedione AMPA antagonists. *Restor Neurol Neuros* **2000,** 17, 45-59.
19. Ruscheweyh, R.; Sandkuhler, J. Role of kainate receptors in nociception. *Brain Res Brain Res Rev* **2002,** 40, 215-22.
20. Naur, P.; Vestergaard, B.; Skov, L. K.; Egebjerg, J.; Gajhede, M.; Kastrup, J. S. Crystal structure of the kainate receptor GluR5 ligand-binding core in complex with (S)-glutamate. *FEBS Lett* **2005,** 579, 1154-60.
21. Kabsch, W. Xds. *Acta Crystallogr D Biol Crystallogr* **2010,** 66, 125-32.
22. Winn, M. D.; Ballard, C. C.; Cowtan, K. D.; Dodson, E. J.; Emsley, P.; Evans, P. R.; Keegan, R. M.; Krissinel, E. B.; Leslie, A. G.; McCoy, A.; McNicholas, S. J.; Murshudov, G. N.; Pannu, N. S.; Potterton, E. A.; Powell, H. R.; Read, R. J.; Vagin, A.; Wilson, K. S. Overview of the CCP4 suite and current developments. *Acta Crystallogr D Biol Crystallogr* **2011,** 67, 235-42.
23. McCoy, A. J.; Grosse-Kunstleve, R. W.; Adams, P. D.; Winn, M. D.; Storoni, L. C.; Read, R. J. Phaser crystallographic software. *J Appl Crystallogr* **2007,** 40, 658-674.
24. Adams, P. D.; Afonine, P. V.; Bunkoczi, G.; Chen, V. B.; Davis, I. W.; Echols, N.; Headd, J. J.; Hung, L. W.; Kapral, G. J.; Grosse-Kunstleve, R. W.; McCoy, A. J.; Moriarty, N. W.; Oeffner, R.; Read, R. J.; Richardson, D. C.; Richardson, J. S.; Terwilliger, T. C.; Zwart, P. H. PHENIX: a comprehensive Python-based system for macromolecular structure solution. *Acta Crystallogr D Biol Crystallogr* **2010,** 66, 213-21.
25. Moriarty, N. W.; Grosse-Kunstleve, R. W.; Adams, P. D. electronic Ligand Builder and Optimization Workbench (eLBOW): a tool for ligand coordinate and restraint generation. *Acta Crystallogr D Biol Crystallogr* **2009,** 65, 1074-80.
26. Emsley, P.; Lohkamp, B.; Scott, W. G.; Cowtan, K. Features and development of Coot. *Acta Crystallogr D Biol Crystallogr* **2010,** 66, 486-501.
27. Hayward, S.; Lee, R. A. Improvements in the analysis of domain motions in proteins from conformational change: DynDom version 1.50. *J Mol Graph Model* **2002,** 21, 181-3.
28. Krissinel, E.; Henrick, K. Inference of macromolecular assemblies from crystalline state. *J Mol Biol* **2007,** 372, 774-97.
29. Assaf, Z.; Larsen, A. P.; Venskutonyte, R.; Han, L.; Abrahamsen, B.; Nielsen, B.; Gajhede, M.; Kastrup, J. S.; Jensen, A. A.; Pickering, D. S.; Frydenvang, K.; Gefflaut, T.; Bunch, L. Chemoenzymatic synthesis of new 2,4-syn-functionalized (S)-glutamate analogues and structure-activity relationship studies at ionotropic glutamate receptors and excitatory amino acid transporters. *J Med Chem* **2013,** 56, 1614-28.
30. Alcaide, A.; Marconi, L.; Marek, A.; Haym, I.; Nielsen, B.; Møllerud, S.; Jensen, M.; Conti, P.; Pickering, D. S.; Bunch, L. Synthesis and pharmacological characterization of the selective GluK1 radioligand (S)-2-amino-3-(6-[3H]-2,4-dioxo-3,4-dihydrothieno[3,2-d]pyrimidin-1(2H)-yl)propanoic acid ([3H]-NF608). *Med. Chem. Commun.* **2016,** 7, 9.
31. Møllerud, S.; Kastrup, J. S.; Pickering, D. S. A pharmacological profile of the high-affinity GluK5 kainate receptor. *Eur J Pharmacol* **2016,** 788, 315-320.
32. Sagot, E.; Pickering, D. S.; Pu, X.; Umberti, M.; Stensbol, T. B.; Nielsen, B.; Chapelet, M.; Bolte, J.; Gefflaut, T.; Bunch, L. Chemo-enzymatic synthesis of a series of 2,4-syn-functionalized (S)-glutamate analogues: new insight into the structure-activity relation of ionotropic glutamate receptor subtypes 5, 6, and 7. *J Med Chem* **2008,** 51, 4093-103.

33. Krintel, C.; Frydenvang, K.; Ceravalls de Rabassa, A.; Kaern, A. M.; Gajhede, M.; Pickering, D. S.; Kastrup, J. S. L-Asp is a useful tool in the purification of the ionotropic glutamate receptor A2 ligand-binding domain. *FEBS J* **2014,** 281, 2422-30.
34. Venskutonyte, R.; Larsen, A. P.; Frydenvang, K.; Gajhede, M.; Sagot, E.; Assaf, Z.; Gefflaut, T.; Pickering, D. S.; Bunch, L.; Kastrup, J. S. Molecular recognition of two 2,4-syn-functionalized (S)-glutamate analogues by the kainate receptor GluK3 ligand binding domain. *ChemMedChem* **2014,** 9, 2254-9.
35. Zimmermann, M. Ethical guidelines for investigations of experimental pain in conscious animals. *Pain* **1983,** 16, 109-10.

TOC graphic: For table of contents use only

"N-(7-(1H-imidazol-1-yl)-2,3-dioxo-6-(trifluoromethyl)-3,4-dihydroquinoxalin-1(2H)-yl)benzamide - a new kainate receptor selective antagonist and analgesic: Synthesis, X-ray crystallography, structure-affinity relationships, in vitro and in vivo pharmacology"

Stine Møllerud, Rie B. Hansen, Jakob Pallesen, Piero Temperini, Diletta Pasini, Jan Bornholt, Birgitte Nielsen, Esmira Mamedova, Paulina Chalupnik, Ana V. Paternain, Juan Lerma, Marta Diaz del Castillo, Jesper T. Andreasen, Karla Frydenvang, Jette S. Kastrup, Tommy N. Johansen and Darryl S. Pickering.

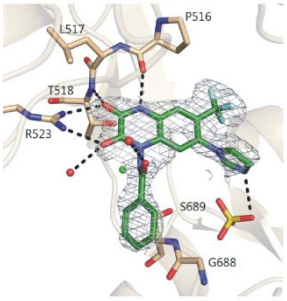

11 in the GluK1 LBD

Table of Content (TOC)

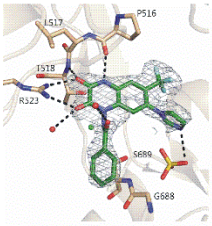

11 in the GluK1 LBD

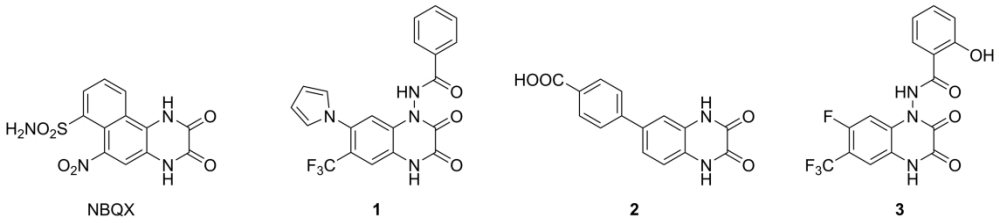

Figure 1

137x30mm (600 x 600 DPI)

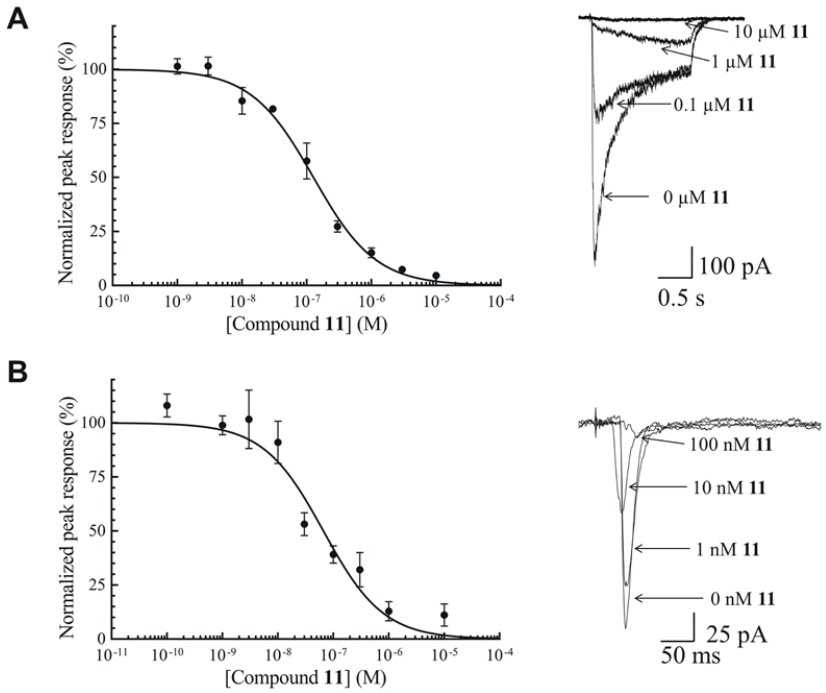

Figure 2

254x190mm (96 x 96 DPI)

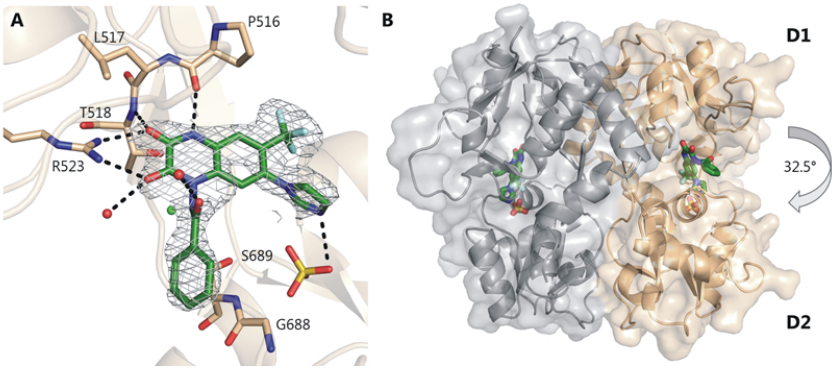

Figure 3

254x190mm (96 x 96 DPI)

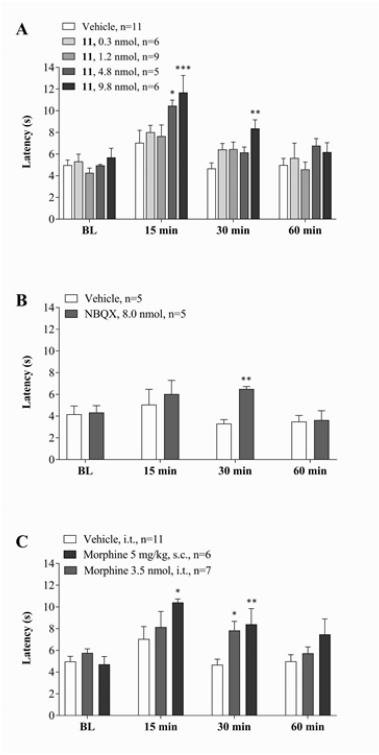

Figure 4

254x190mm (96 x 96 DPI)

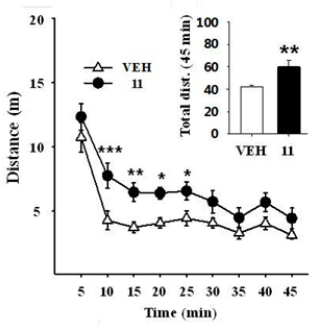

Figure 5

254x190mm (96 x 96 DPI)

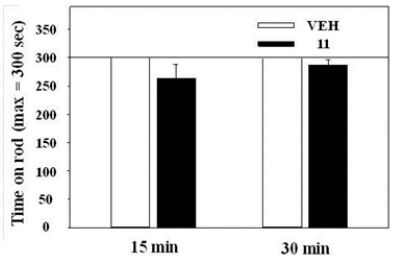

Figure 6

254x190mm (96 x 96 DPI)

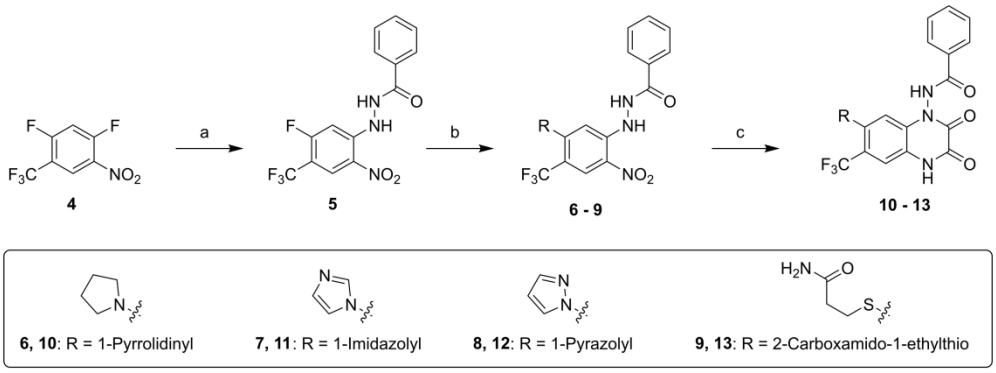

Scheme 1

138x51mm (600 x 600 DPI)

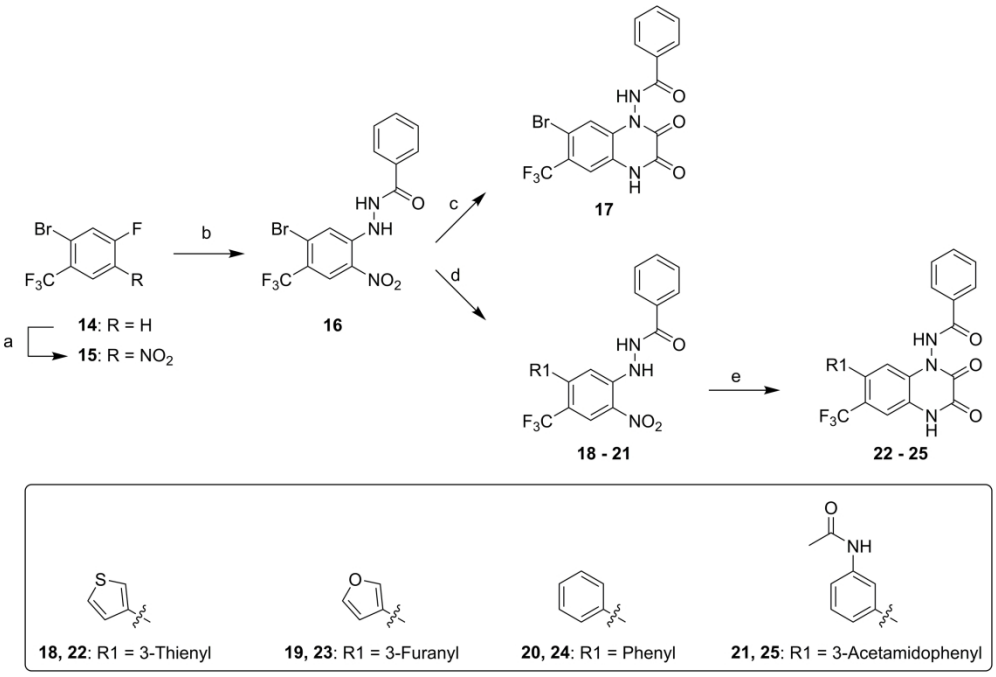

Scheme 2

131x89mm (600 x 600 DPI)